Nonlinear Dyn (2020) 102:635–642
https://doi.org/10.1007/s11071-020-05893-z

ORIGINAL PAPER

Resonance induced by mixed couplings in a three-node motif

Cong Liu · Xiyun Zhang · Xiaoming Liang

Received: 28 February 2020 / Accepted: 12 August 2020 / Published online: 20 August 2020

Abstract Inspired by the coexistence of excitatory and inhibitory neurons in real neural networks, we propose a motif of three coupled nodes, one with positive coupling and two with negative couplings, for signal amplification. Utilizing the bistable overdamped oscillator as well as the excitable neuron models, we show that the response of the motif is optimized for an intermediate range of coupling strength, i.e., coupling-induced resonance. Through theoretical analyses, we find that the underlying mechanism for the resonance is an abrupt pitchfork bifurcation caused by the mixed positive and negative couplings.

Keywords Signal amplification · Bistable overdamped oscillator · Excitable neuron · Mixed couplings · Motif · Pitchfork bifurcation

1 Introduction

Diverse animals possess particular sensory system that can efficiently detect and response to external signals, even when the signals are weak [1–3]. For example, a crayfish can sensor perturbations in the surrounding environment caused by nearby predators [4], and a fox can hear the footsteps of mice under the snow [5]. In order to understand these natural phenomena, as well as for relevant bionic applications, it has become an important field in neuroscience of understanding the origin of the ability for a sensory system to detect weak signals [6–10].

At the single neuron level, researchers have discovered that additional noise to an excitable neuron can improve the detectability to a faint signal under certain conditions. Such an noise-induced improvement may arise from the effect known as stochastic resonance (SR)—adding noise with suitable intensity makes a weak signal accessible for an excitable neuron [11–13]. This additional noise may originate from environmental fluctuations or biochemical and electrical activities [7,14]. Notably, noise with neither strong nor small intensity can lead to stochastic resonance. For small additional noise, the weak signal cannot be raised enough to fire the sensory neuron, while too strong noise will overwhelm the signal which leads to random firings of the sensory neuron. In contrast, intermediate noise may trigger the sensory neuron to fire with a rhythm matching the period of the driving signal, which leads to an enhanced response. At the neuronal population level, the SR response of a single neuron can be further enhanced when coupled into an neuron array, which is known as array-enhanced SR [15–17]. However, in most natural systems, neurons are organized through complex networks whose structures are

C. Liu · X. Liang (✉)
School of Physics and Electronic Engineering, Jiangsu Normal University, Xuzhou 221116, China
e-mail: xm-liang@hotmail.com

X. Zhang
Department of Physics, Jinan University, Guangzhou 510632, Guangdong, China

neither purely random nor regular [18–21]. It has been shown that the structure of coupling networks significantly affects SR. For instance, small-world networks with a small fraction of long-range links can lead to a great improvement in SR [22,23]; scale-free networks with hubs can amplify weak signals even without the aid of additional noise, i.e., amplified signal response is purely induced by star-like structure [24–26].

Recent efforts to understand signal amplification focused on the effect of quenched noise inherent in the neuronal populations [27–29]. In particular, the diversity of network interactions plays an important role on the performance of signal amplification, which is closer to realistic cases since neuronal networks are highly heterogeneous in their connections [30–33]. Remarkably, not only heterogeneity from network topology can enhance signal amplification, but also heterogeneous couplings can trigger resonance behavior. As one of the most updated development, Liu et al. found that mixed weighted positive and negative couplings in an ensemble of bistable overdamped oscillators can enhance signal response in a form of coupling-induced resonance [34]. With further analyses, they showed that in the presence of mixed positive and negative couplings, the oscillator population spontaneously splits into three clusters—two with negative couplings and one with positive coupling, and the enhanced resonance shows significant association with the coordinated oscillations of these three clusters. Although a three-cluster model was proposed to explain the origin of the observed resonance, the underlying dynamic mechanism remains unclear.

In this paper, we present an abrupt pitchfork bifurcation mechanism for this recently revealed coupling-induced resonance. Specifically, we introduce a three-node motif comprises two negatively coupled nodes and one positively coupled node as a minimal case for the three-cluster model. We investigate the response of this three-node motif to an external subthreshold signal and find a well-reproduced coupling-induced resonance. We also show that with an increase in coupling strength the motif undergoes an abrupt pitchfork bifurcation which causes a dynamical transition from small-amplitude oscillations to large-amplitude oscillations, leading to the onset of resonance. This finding implies that sensory systems could benefit from the natural coupling diversity to optimize their responses to weak external signals.

2 Models and results

2.1 Bistable overdamped model

In this section, we consider a motif of three bistable overdamped oscillators, described by

$$\dot{x}_i = x_i - x_i^3 + \frac{c_i}{3}\sum_{j=1}^{3}(x_j - x_i) + A\sin(\omega t), \quad i = 1, 2, 3, \tag{1}$$

where c_i represents the oscillator-dependent coupling. The oscillator i acts attractively for $c_i > 0$ and repulsively for $c_i < 0$. According to the three-cluster model [34], we set the couplings of the three oscillators in the motif (1) as

$$\begin{pmatrix} c_1 \\ c_2 \\ c_3 \end{pmatrix} = \begin{pmatrix} c \\ -c \\ -c \end{pmatrix}, \tag{2}$$

where $c \geq 0$ denotes the coupling strength.

Without coupling, i.e., $c = 0$, each oscillator in motif (1) can generate two distinct responses to the external signal $A\sin(\omega t)$ depending on the signal amplitude A. For $A > A_c \approx 0.39$ each oscillator can oscillate about its unstable fixed point $x^u = 0$, while for $A < A_c$ they only jiggle around one of the two stable fixed points $x^s = \pm 1$. Following [34], a subthreshold signal with amplitude $A = 0.3$ and frequency $\omega = \pi/50$ is considered, and the initial conditions of the oscillators are set as

$$\begin{pmatrix} x_1(0) \\ x_2(0) \\ x_3(0) \end{pmatrix} = \begin{pmatrix} \pm 1 \\ \pm 1 \\ \mp 1 \end{pmatrix}. \tag{3}$$

Notably, it is required that the two oscillators with negative couplings are set with different initial conditions for signal amplification, but no specific requirement for the oscillator with positive coupling.

To quantify the response of the motif to the external signal, we apply the spectral amplification factor defined as [27]

$$\eta = \frac{4}{A^2}\left|\left\langle e^{i\omega t} X(t)\right\rangle\right|^2. \tag{4}$$

where $X(t) = (x_1(t) + x_2(t) + x_3(t))/3$ denotes the global dynamics of the motif and $\langle\cdot\rangle$ stands for the time average.

Figure 1a shows the spectral amplification factor η versus coupling strength c, which exhibits a bell-shaped structure with a jump at a critical coupling strength

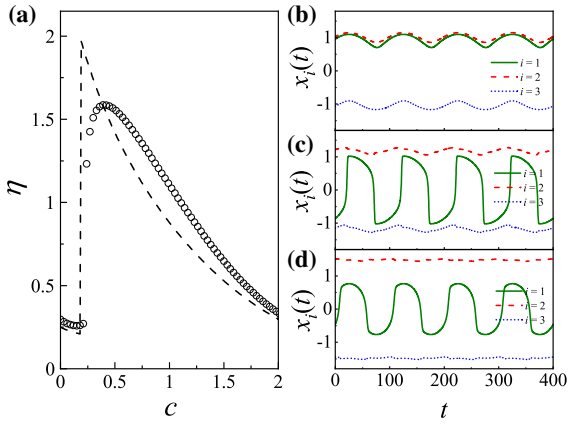

Fig. 1 (Color online) Left: **a** The spectral amplification factor η of Eq. (1) versus coupling strength c, where the dashed line denotes the prediction of Eqs. (22)–(24). Right: Time series $x_i(t)$ of Eq. (1) for **b** $c = 0.1$, **c** $c = 0.4$, and **d** $c = 1.2$, where the green solid lines, red dashed lines, and blue dotted lines represent $x_1(t)$, $x_2(t)$, and $x_3(t)$, respectively

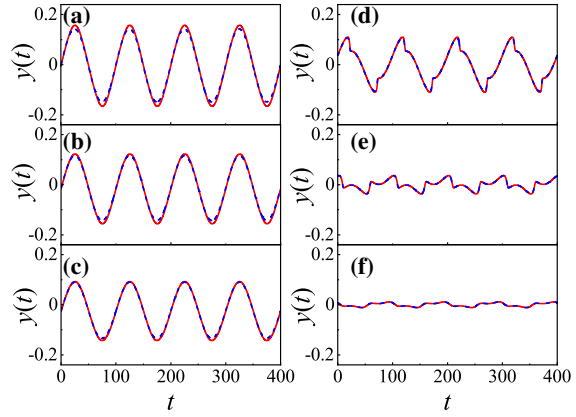

Fig. 2 (Color online) Time series $y(t)$ of Eqs. (6) and (9) for **a** $c = 0.02$, **b** $c = 0.1$, **c** $c = 0.2$, **d** $c = 0.4$, **e** $c = 1.2$, and **f** $c = 2$, where the red solid lines, blue dashed lines represent Eqs. (6) and (9), respectively

$c_1 \approx 0.23$. Figure 1b–d further shows the oscillation waves of the three oscillators for different coupling strengths. One can observe a dynamical transition at the critical coupling strength $c = c_1$. For $c < c_1$ there exist only two oscillation clusters with small amplitudes. When the coupling strength is beyond c_1, the positively coupled oscillator (the first oscillator) separates from the previous clusters and forms the third oscillation cluster with a much larger amplitude. Due to its large oscillation amplitude, the behavior of the first oscillator dominates the global dynamics of the motif. This process is in agreement with the coupling-induced resonance observed in Ref. [34], and thus, our three-node motif is able to reproduce both the resonance and the dynamical transition of the network.

To understand the observed resonance in the three-node motif, we define $y = (x_2 + x_3)/2$ and $z = (x_2 - x_3)/2$ as the mean dynamics and synchronization error of the two oscillators with negative couplings, respectively. Then, Eq. (1) can be rewritten as

$$\dot{x}_1 = \left(1 - \frac{2c}{3}\right) x_1 - x_1^3 + \frac{2c}{3} y + A\sin(\omega t), \quad (5)$$

$$\dot{y} = \left(1 + \frac{c}{3} - 3z^2\right) y - y^3 - \frac{c}{3} x_1 + A\sin(\omega t), \quad (6)$$

$$\dot{z} = (1 + c - 3y^2)z - z^3. \quad (7)$$

Since the second and third oscillators with negative couplings have relatively smaller amplitudes comparing to the first one, we may assume $\dot{y} = \dot{z} = 0$. For $\dot{z} = 0$, we get $z = 0$ and $z^2 = 1 + c - 3y^2$. According to Fig. 1b–d, the two oscillators ($i = 2, 3$) with negative couplings repel each other, indicating that the root $z = 0$ cannot be physically observed. Substituting $z^2 = 1 + c - 3y^2$ into Eq. (6) with the assumption $\dot{y} = 0$ yields

$$-\frac{6 + 8c}{3} y + 8y^3 - \frac{c}{3} x_1 + A\sin(\omega t) = 0. \quad (8)$$

Since y is a small fluctuation, the cubic term y^3 can be neglected in Eq. (8), leading to

$$y = \frac{3A\sin(\omega t) - c x_1}{6 + 8c}. \quad (9)$$

Figure 2 shows the results of Eq. (9) for different coupling strengths, which provide a good approximation to the numerical data of Eq. (6). This indicates that $\dot{z} = 0$, $\dot{y} = 0$ and $y^3 \approx 0$ are reasonable approximations. From Eq. (9), the global dynamics can be expressed as

$$X(t) = \frac{x_1 + 2y}{3} = \frac{1 + c}{3 + 4c} x_1 + \frac{A}{3 + 4c}\sin(\omega t). \quad (10)$$

Substituting Eq. (9) into Eq. (5) obtains

$$\dot{x}_1 = \alpha x_1 - x_1^3 + \beta\sin(\omega t), \quad (11)$$

where $\alpha = (3 + 2c - 3c^2)/(3 + 4c)$ and $\beta = A(3 + 5c)/(3 + 4c)$. Without periodic force, i.e., $A = 0$, Eq. (11) undergoes a pitchfork bifurcation as c increases, where the bifurcation point is at $c_2 = (1 + \sqrt{10})/3$. Figure 3a shows the bifurcation diagram of the stable fixed points $\langle x_1 \rangle$ (oscillation centers) as

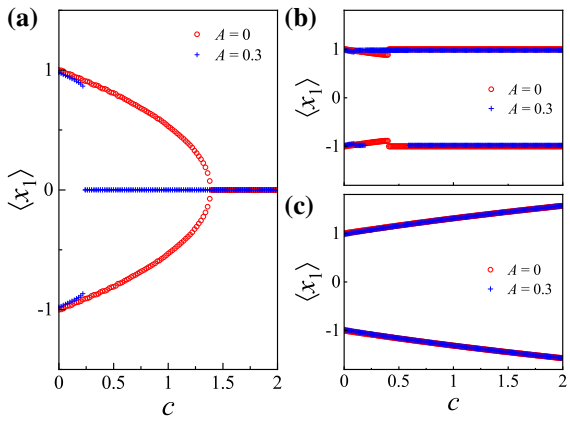

Fig. 3 (Color online) **a** The bifurcation diagram of Eq. (11) at $A = 0$ and $A = 0.3$, respectively. **b**, **c** The bifurcation diagram of Eq. (1) with purely positive ($c_i > 0$) and purely negative ($c_i < 0$) couplings, respectively. The stable fixed points $\langle x_1 \rangle$ are calculated by time average over $200T$ ($T = 2\pi/\omega$) with different initial conditions

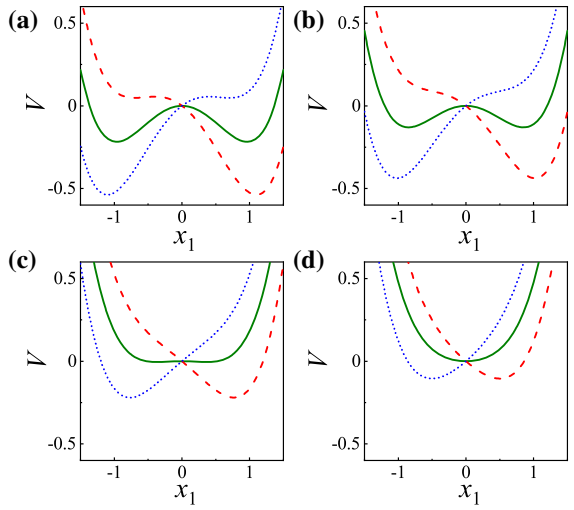

Fig. 4 (Color online) The potential function of Eq. (12) for different coupling strengths. **a** $c = 0.1$, **b** $c = 0.4$, **c** $c = 1.2$, and (d) $c = 2$. The solid lines, dashed lines, and dotted lines denote the potential function at $t = 0$, $t = \pi/2\omega$, and $t = 3\pi/2\omega$, respectively

a function of coupling c, where $\langle x_1 \rangle$ is the time average of $x_1(t)$ over $200T$ ($T = 2\pi/\omega$) with different initial conditions. As c approaches c_2, the two stable fixed points $\langle x_1 \rangle = \pm\sqrt{\alpha}$ move towards each other, and eventually merge into one stable fixed point $\langle x_1 \rangle = 0$ when $c \geq c_2$. In the presence of periodic forcing, i.e., $A = 0.3$, the bifurcation behaves similar as $A = 0$ until $c \approx 0.23$ which is just the critical coupling strength c_1 shown in Fig. 1a. When c reaches c_1, the two stable fixed points abruptly lose their stability dropping into the stable fixed point $x_1^s = 0$, suggesting that c_1 is the abrupt pitchfork bifurcation point. For better comparison, Fig. 3b and c shows the bifurcation diagram of Eq. (1) with purely positive ($c_i > 0$) and purely negative ($c_i < 0$) couplings, respectively. In both of these cases, two fixed points remain stable with c increasing, so the first oscillator keeps jiggling around one of them. This explains the small responses of the network with purely positive and negative couplings shown in Ref. [34]. Therefore, mixed positive and negative couplings cause the stable fixed points to lose stability, initiating the dynamical transition and the coupling-induced resonance.

In order to investigate how the abrupt bifurcation affects signal amplification, we show in Fig. 4 the potential function of Eq. (11) for different coupling strengths, where the potential function is defined as

$$V = -\frac{\alpha}{2}x_1^2 + \frac{1}{4}x_1^4 - \beta x_1 \sin(\omega t). \tag{12}$$

When c is small, e.g., $c = 0.1$, the potential function is W-shaped with two wells and one barrier in the middle (Fig. 4a). Under periodic forcing, the wells periodically rise and fall but maintaining the barrier. The particle to overcome it from one well to the other needs to consume more energy, so that it always stays within one well. After the bifurcation point, e.g., $c = 0.4$, the potential barrier periodically disappears and the width of the well bottom still remains, which leads to produce the large amplitude of oscillation. When the coupling is large, e.g., $c = 1.2$, the potential function changes from W-shape to U-shape with only one well, and the width of well bottom become narrow, which leads to the amplitude of oscillation becomes small. With further increasing coupling strength, e.g., $c = 2$, the well of the U-shaped potential function becomes narrow and steep. Comparing to both the small and large coupling, the potential function at $c = 0.4$, near the bifurcation point c_1, allows a wider range of oscillation leading to the resonance signal amplification.

To analytically get the pitchfork bifurcation point c_1, we consider $\mathrm{d}V/\mathrm{d}x_1 = 0$ at $t = \pm\pi/2\omega$, since the potential barrier is much lower at the maximum (minimum) of the periodic signal. Then, Eq. (12) reduces to a cubic equation as

$$\alpha x_1 - x_1^3 \pm \beta = 0. \tag{13}$$

At the bifurcation point $c = c_1$, Eq. (13) has two equal roots which results in

$$\left(\frac{\beta}{2}\right)^2 = \left(\frac{\alpha}{3}\right)^3. \tag{14}$$

Thus, the pitchfork bifurcation point c_1 obeys the following relationship as

$$\frac{27A^2}{4} = \frac{(3+2c-3c^2)^3}{(3+4c)(3+5c)^2}. \tag{15}$$

From Eq. (15), the pitchfork bifurcation point only depends on the signal amplitude A, which decreases with A. For $A = 0.3$, Eq. (15) analytically gives the pitchfork bifurcation point $c_* \approx 0.18$, which is close to the numerical result $c_1 \approx 0.23$. The difference between our estimate c_* and the numerical result c_1 is due to the assumption $\dot{y} = 0$, since the analytical y, i.e., Eq. (9), obtained from $\dot{y} = 0$ is smaller than the numerical result for $c < c_1$.

When $c < c_*$, the potential barrier remains and the periodic signal $\beta \sin(\omega t)$ is subthreshold. Thus, the first oscillator vibrates around one of the stable points. Assuming $\delta(t)$ as the vibration, then we can write $x_1(t) = \langle x_1 \rangle + \delta(t)$, where $\langle x_1 \rangle = \pm\sqrt{\alpha}$ are the stable fixed points in the absence of periodic forcing ($A = 0$). Inserting $x_1(t)$ into Eq. (11) and neglecting $\delta(t)^2$ and $\delta(t)^3$, the dynamical equation of the vibration can be simplified as

$$\dot{\delta}(t) = -2\alpha\delta(t) + \beta \sin(\omega t). \tag{16}$$

This is a linear differential equation of first order, and its solution is given by

$$\delta(t) \approx -\frac{\beta\omega}{4\alpha^2+\omega^2}\cos(\omega t) + \frac{2\beta}{4\alpha^2+\omega^2}\sin(\omega t). \tag{17}$$

Then, the approximate solution of Eq. (11) is

$$x_1(t) = \pm\sqrt{\alpha} + \frac{\beta}{\sqrt{\omega^2+4\alpha^2}}\sin(\omega t - \phi), \tag{18}$$

where $\tan\phi = \omega/2\alpha$ denotes the phase shift.

On the other hand, when $c \geq c_*$ the potential barrier disappears and the periodic signal $\beta \sin(\omega t)$ becomes suprathreshold. In this situation, the approximate solution of Eq. (11) for $c_* \leq c < c_2$ can be obtained by assuming the signal frequency ω is sufficient small. Then, the periodic forcing $\beta \sin(\omega t)$ can be taken as a constant $\pm\beta$. Thus, the oscillation amplitude of x_1 can be approximately solved from the reduced equation $\alpha x_1 - x_1^3 \pm \beta = 0$, which is

$$2\sqrt{\frac{\alpha}{3}}\cosh\left(\frac{1}{3}\operatorname{arcosh}\left(\frac{3\beta}{2\alpha}\sqrt{\frac{3}{\alpha}}\right)\right). \tag{19}$$

Assuming the first oscillator oscillates with a sine wave, then its dynamics equitation can be expressed as

$$x_1(t) = 2\sqrt{\frac{\alpha}{3}}\cosh\left(\frac{1}{3}\operatorname{arcosh}\left(\frac{3\beta}{2\alpha}\sqrt{\frac{3}{\alpha}}\right)\right)\sin(\omega t). \tag{20}$$

Similarly, for $c \geq c_2$ the dynamics equitation of x_1 is

$$x_1(t) = 2\sqrt{-\frac{\alpha}{3}}\sinh\left(\frac{1}{3}\operatorname{arsinh}\left(-\frac{3\beta}{2\alpha}\sqrt{-\frac{3}{\alpha}}\right)\right)\sin(\omega t). \tag{21}$$

Putting Eqs. (18) and (20)–(21) into Eq. (10) and combining Eq. (4), we can analytically obtain the response of the motif. Specifically, when $c < c_*$, the spectral amplification factor is

$$\eta = \frac{(c^2-12c-9)^2 + (3+4c)^2\omega^2}{4(3+4c)^2(3+2c-3c^2)^2 + (3+4c)^4\omega^2}, \tag{22}$$

which is independent of the signal amplitude A. When $c_* \leq c < c_2$, the spectral amplification factor is

$$\eta = \frac{\left((1+c)2\sqrt{\frac{\alpha}{3}}\cosh\left(\frac{1}{3}\operatorname{arcosh}\left(\frac{3\beta}{2\alpha}\sqrt{\frac{3}{\alpha}}\right)\right) + A\right)^2}{(3+4c)^2A^2}, \tag{23}$$

and for $c \geq c_2$, the spectral amplification factor becomes

$$\eta = \frac{\left((1+c)2\sqrt{-\frac{\alpha}{3}}\sinh\left(\frac{1}{3}\operatorname{arsinh}\left(-\frac{3\beta}{2\alpha}\sqrt{-\frac{3}{\alpha}}\right)\right) + A\right)^2}{(3+4c)^2A^2}. \tag{24}$$

Figure 1a shows the theoretical result of Eqs. (22)–(24), which predicts well with the numerical result come from Eq. (1), except for the intermediate coupling. The main reason for this deviation is that the square-like wave of $x_1(t)$ is approximately represented as the sine wave around c_1 (Fig. 1c, d).

2.2 Excitable neuron model

To verify the above results in a more biologically realistic framework, we replace the bistable overdamped oscillator by the FitzHugh–Nagumo (FHN) neuron

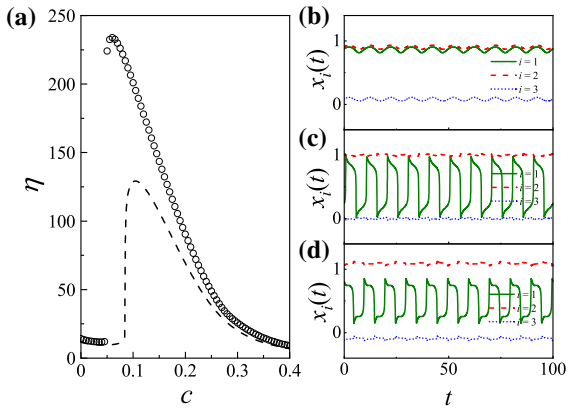

Fig. 5 (Color online) Left: **a** The spectral amplification factor η of Eq. (25) versus coupling strength c, where the dashed line denotes the prediction of Eq. (28). Right: Time series $x_i(t)$ of Eq. (25) for **b** $c = 0.02$, **c** $c = 0.1$, and **d** $c = 0.2$, where the green solid lines, red dashed lines, and blue dotted lines represent $x_1(t)$, $x_2(t)$, and $x_3(t)$, respectively

model [35,36]. Then, the governing equations for the motif becomes

$$\begin{aligned}\varepsilon\dot{x}_i &= x_i(1-x_i)(x_i-a) - y_i + \frac{c_i}{3}\sum_{j=1}^{3}(x_j - x_i) \\ &\quad + A\sin(\omega t), \\ \dot{y}_i &= bx_i - y_i - d,\ i = 1, 2, 3,\end{aligned} \tag{25}$$

where x_i and y_i represent the fast and slow variables respectively. $\varepsilon = 0.01$, $a = 0.5$, $b = 0.1$, $d = 0.05$ are applied. With this setup, the FitzHugh–Nagumo neuron model is bistable and excitable, which has two stable fixed points as $(x_1^s, y_1^s) = (0.11, -0.04)$ and $(x_2^s, y_2^s) = (0.89, 0.04)$. Similarly, the couplings of neurons are set the same as in Eq. (2), and their initial conditions are assigned as follows:

$$\begin{pmatrix} x_1(0), & y_1(0) \\ x_2(0), & y_2(0) \\ x_3(0), & y_3(0) \end{pmatrix} = \begin{pmatrix} 0.89, & 0.04 \\ 0.89, & 0.04 \\ 0.11, & -0.04 \end{pmatrix}, \tag{26}$$

where two neurons with negative couplings are also required to have different initial conditions. To model a subthreshold signal, the amplitude and frequency of the external input are set as $A = 0.01$ and $\omega = \pi/5$, respectively [36]. For simplicity, the response of the motif to the external signal is estimated by the global dynamics of the fast variables, i.e., $X = (x_1 + x_2 + x_3)/3$.

Figure 5a shows a similar resonance dependence of the spectra amplification factor η on the coupling strength c. Meanwhile, an abrupt jump of η occurs at a critical coupling strength $c_3 \approx 0.05$. Time series of $x_i(t)$ shown in Fig. 5b–d further indicate a dynamical transition at $c = c_3$—from the case of two oscillation clusters with small amplitudes to the case of three oscillation clusters. Analogously, when $c \geq c_3$ the positively coupled neuron dominates the global dynamics due to its large-amplitude firings.

To analyze the resonance behavior, we rewrite Eq. (25) as

$$\begin{aligned}\varepsilon\dot{x}_1 &= x_1(1-x_1)(x_1-a) - y_1 + \frac{2c}{3}(M_x - x_1) \\ &\quad + A\sin(\omega t), \\ \dot{y}_1 &= bx_1 - y_1 - d, \\ \varepsilon\dot{M}_x &= \left(-a - 3D_x^2 + \frac{c}{3}\right)M_x - (a+1)(M_x^2 + D_x^2) \\ &\quad - M_x^3 - M_y - \frac{c}{3}x_1 + A\sin(\omega t), \\ \dot{M}_y &= bM_x - M_y - d, \\ \varepsilon\dot{D}_x &= \left(c - a - 3M_x^2 + 2(a+1)M_x\right)D_x - D_x^3 - D_y, \\ \dot{D}_y &= bD_x - D_y,\end{aligned} \tag{27}$$

where the definitions $M_x = (x_2 + x_3)/2$, $M_y = (y_2 + y_3)/2$, $D_x = (x_2 - x_3)/2$, and $D_y = (y_2 - y_3)/2$ are used. Notably, D_x is a small value for the two negatively coupled neurons (Fig. 5b–d), and thus, we assume $\dot{D}_x = 0$. Since the dynamics of the slow variables can be considered as constants comparing to the fast variables, we also assume that the slow variables satisfy $\dot{y}_1 = 0$, $\dot{M}_y = 0$, and $\dot{D}_y = 0$. Providing these assumptions, Eq. (27) can be reduced to

$$\begin{aligned}\varepsilon\dot{x}_1 &= x_1(1-x_1)(x_1-a) - bx_1 + d \\ &\quad + \frac{2c}{3}(M_x - x_1) + A\sin(\omega t), \\ \varepsilon\dot{M}_x &= \left(2a + 2b - \frac{8c}{3} + 2(a+1)^2\right)M_x \\ &\quad - 8(a+1)M_x^2 + 8M_x^3 + d - \frac{c}{3}x_1 \\ &\quad + (a+1)(c - a - b) + A\sin(\omega t).\end{aligned} \tag{28}$$

Equation (28) describes a system of two coupled neurons, one (x_1) acts attractively ($c_i > 0$) while the other (M_x) acts repulsively ($c_i < 0$). Figure 6a plots the bifurcation diagram of the stable fixed points $\langle x_1 \rangle$ of Eq. (28) with $A = 0$ and $A = 0.01$, respectively. For $A = 0$, the two stable fixed points approach each other, and merge at $c_4 = 0.2$, remaining a fixed point $\langle x_1 \rangle = 0.5$. For $A = 0.01$, the system undergoes an abrupt pitchfork bifurcation at $c \approx 0.08$, leading to the

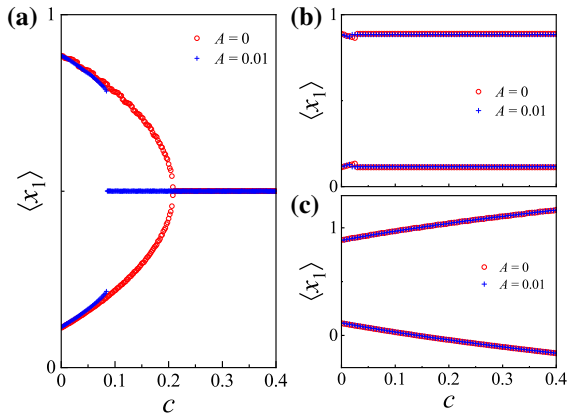

Fig. 6 (Color online) **a** The bifurcation diagram of Eq. (28) at $A = 0$ and $A = 0.01$, respectively. **b**, **c** The bifurcation diagram of Eq. (25) with purely positive ($c_i > 0$) and purely negative ($c_i < 0$) couplings, respectively. The stable fixed points $\langle x_1 \rangle$ are calculated by time average over $200T$ ($T = 2\pi/\omega$) with different initial conditions

occurrence of the resonance as well as the dynamical transition at $c_3 = 0.05$. This means the pitchfork bifurcation point c_3 decreases with the increase in the amplitude A. Meanwhile, Fig. 6b and c shows the bifurcation diagram of $x_1(t)$ in Eq. (25) for both purely positive couplings and purely negative couplings, respectively. Similarly, two fixed points remain stable for $A = 0$ and $A = 0.01$ as c increases. Collectively, only mixed positive and negative couplings can cause an abrupt pitchfork bifurcation, which leads to the coupling-induced resonance. Finally, we insert $X = (x_1 + 2M_x)/3$ obtained from Eq. (28) into Eq. (4) to evaluate the analytical spectral amplification factor η. Figure 5a shows the result, which is approximately consistent with the resonance behavior of Eq. (25). Note that the deviation of Eq. (28) is large in the intermediate coupling and we attribute this to the approximations of $\dot{D}_x = 0$, $\dot{y}_1 = 0$, $\dot{M}_y = 0$, and $\dot{D}_y = 0$.

3 Conclusions

In conclusion, we have investigated the response of a three-node motif with mixed attractive and repulsive couplings to a weak external signal. We have found that this simple motif can generate a bell-shaped resonance on the coupling strength. We have revealed that such coupling-induced resonance is the consequence of an abrupt pitchfork bifurcation induced by the mixed positive and negative couplings. We have also shown that this abrupt bifurcation cannot appear for both the purely positive couplings as well as the purely negative couplings. We have also demonstrated the mechanism of mixed coupling-induced resonance works efficiently for both the bistable overdamped oscillators and the excitable neuron models. On the one hand, these findings lead us to a speculation that the instability and dynamical phase transition caused by mixed couplings could be an efficient mechanism for processing information in sensory systems, since heterogeneous interactions are common in natural systems. On the other hand, small motifs are easy to build and control; thus, our findings may also provide new insights on the design of simple but efficient artificial devices.

Acknowledgements X.L. was supported by the NNSF of China under Grant No. 11305078. We thank the anonymous reviewers for critical comments that helped improve the paper.

Compliance with ethical standards

Conflict of interest The authors declare that they have no conflict of interest.

References

1. Hänggi, P.: Stochastic resonance in biology how noise can enhance detection of weak signals and help improve biological information processing. ChemPhysChem **3**(3), 285–290 (2002)
2. Schnupp, J.W.H., Carr, C.E.: On hearing with more than one ear: lessons from evolution. Nat. Neurosci. **12**(6), 692 (2009)
3. Fenton, M.B.: The world through a bat's ear. Science **333**(6042), 528–529 (2011)
4. Collins, J.J.: Fishing for function in noise. Nature **402**(6759), 241–242 (1999)
5. McKenna, M.F.: The sounds around us. Phys. Today **73**(1), 28–34 (2020)
6. Deng, B., Wang, J., Wei, X., Tsang, K.M., Chan, W.L.: Vibrational resonance in neuron populations. Chaos **20**(1), 013113 (2010)
7. McDonnell, M.D., Ward, L.M.: The benefits of noise in neural systems: bridging theory and experiment. Nat. Rev. Neurosci. **12**(7), 415–425 (2011)
8. Lü, M., Wang, C., Ren, G., Ma, J., Song, X.: Model of electrical activity in a neuron under magnetic flow effect. Nonlinear Dyn. **85**(3), 1479–1490 (2016)
9. Ma, J., Tang, J.: A review for dynamics in neuron and neuronal network. Nonlinear Dyn. **89**(3), 1569–1578 (2017)
10. Han, X., Zhang, Y., Bi, Q., Kurths, J.: Two novel bursting patterns in the Duffing system with multiple-frequency slow parametric excitations. Chaos **28**(4), 043111 (2018)
11. Gammaitoni, L., Hänggi, P., Jung, P., Marchesoni, F.: Stochastic resonance. Rev. Mod. Phys. **70**(1), 223 (1998)

12. Lindner, B., García-Ojalvo, J., Neiman, A., Schimansky-Geier, L.: Effects of noise in excitable systems. Phys. Rep. **392**(6), 321–424 (2004)
13. Wang, Q., Perc, M., Duan, Z., Chen, G.: Synchronization transitions on scale-free neuronal networks due to finite information transmission delays. Phys. Rev. E **80**(2), 026206 (2009)
14. Liang, X., Dhamala, M., Zhao, L., Liu, Z.: Phase-disorder-induced double resonance of neuronal activity. Phys. Rev. E **82**(1), 010902(R) (2010)
15. Lindner, J.F., Meadows, B.K., Ditto, W.L., Inchiosa, M.E., Bulsara, A.R.: Array enhanced stochastic resonance and spatiotemporal synchronization. Phys. Rev. Lett. **75**(1), 3 (1995)
16. Zhou, C., Kurths, J., Hu, B.: Array-enhanced coherence resonance: nontrivial effects of heterogeneity and spatial independence of noise. Phys. Rev. Lett. **87**(9), 098101 (2001)
17. Pikovsky, A., Zaikin, A., de La Casa, M.A.: System size resonance in coupled noisy systems and in the Ising model. Phys. Rev. Lett. **88**(5), 050601 (2002)
18. Strogatz, S.H.: Exploring complex networks. Nature **410**(6825), 268–276 (2001)
19. Bar-Yam, Y., Epstein, I.R.: Response of complex networks to stimuli. Proc. Natl. Acad. Sci. U.S.A. **101**(13), 4341–4345 (2004)
20. Bullmore, E., Sporns, O.: Complex brain networks: graph theoretical analysis of structural and functional systems. Nat. Rev. Neurosci. **10**(3), 186–198 (2009)
21. Zhou, J., Zhou, Y., Liu, Z.: Amplification of signal response at an arbitrary node of a complex network. Phys. Rev. E **83**(4), 046107 (2011)
22. Gao, Z., Hu, B., Hu, G.: Stochastic resonance of small-world networks. Phys. Rev. E **65**(1), 016209 (2001)
23. Perc, M.: Stochastic resonance on excitable small-world networks via a pacemaker. Phys. Rev. E **76**(6), 066203 (2007)
24. Acebrón, J.A., Lozano, S., Arenas, A.: Amplified signal response in scale-free networks by collaborative signaling. Phys. Rev. Lett. **99**(12), 128701 (2007)
25. Liu, Z., Munakata, T.: Scale-free topology-induced double resonance in networked two-state systems. Phys. Rev. E **78**(4), 046111 (2008)
26. Lu, F., Liu, Z.: Frequency sensitivity of signal detection in scale-free networks. Chin. Phys. Lett. **26**(4), 040503 (2009)
27. Tessone, C.J., Mirasso, C.R., Toral, R., Gunton, J.D.: Diversity-induced resonance. Phys. Rev. Lett. **97**(19), 194101 (2006)
28. Gassel, M., Glatt, E., Kaiser, F.: Doubly diversity-induced resonance. Phys. Rev. E **76**(1), 016203 (2007)
29. Shen, C., Chen, H., Zhang, J.: Amplified signal response by neuronal diversity on complex networks. Chin. Phys. Lett. **25**(5), 1591 (2008)
30. Wu, L., Zhu, S., Luo, X.: Diversity-induced resonance on weighted scale-free networks. Chaos **20**(3), 033113 (2010)
31. Martins, T.V., Livina, V.N., Majtey, A.P., Toral, R.: Resonance induced by repulsive interactions in a model of globally coupled bistable systems. Phys. Rev. E **81**(4), 041103 (2010)
32. Hoge, G.J., Davidson, K.G.V., Yasumura, T., Castillo, P.E., Rash, J.E., Pereda, A.E.: The extent and strength of electrical coupling between inferior olivary neurons is heterogeneous. J. Neurophysiol. **105**(3), 1089–1101 (2011)
33. Liang, X., Zhao, L., Liu, Z.: Optimal signal amplification in weighted scale-free networks. Chaos **22**(2), 023128 (2012)
34. Liu, C., Liang, X.: Resonance induced by coupling diversity in globally coupled bistable oscillators. Phys. Rev. E **100**(3), 032206 (2019)
35. Zaikin, A., García-Ojalvo, J., Báscones, R., Ullner, E., Kurths, J.: Doubly stochastic coherence via noise-induced symmetry in bistable neural models. Phys. Rev. Lett. **90**(3), 030601 (2003)
36. Liang, X., Yanchuk, S., Zhao, L.: Gating-signal propagation by a feed-forward neural motif. Phys. Rev. E **88**(1), 012910 (2013)